Article

Structure

Structural Insights into a Unique Dimeric DEAD-Box Helicase CshA that Promotes RNA Decay

Graphical Abstract

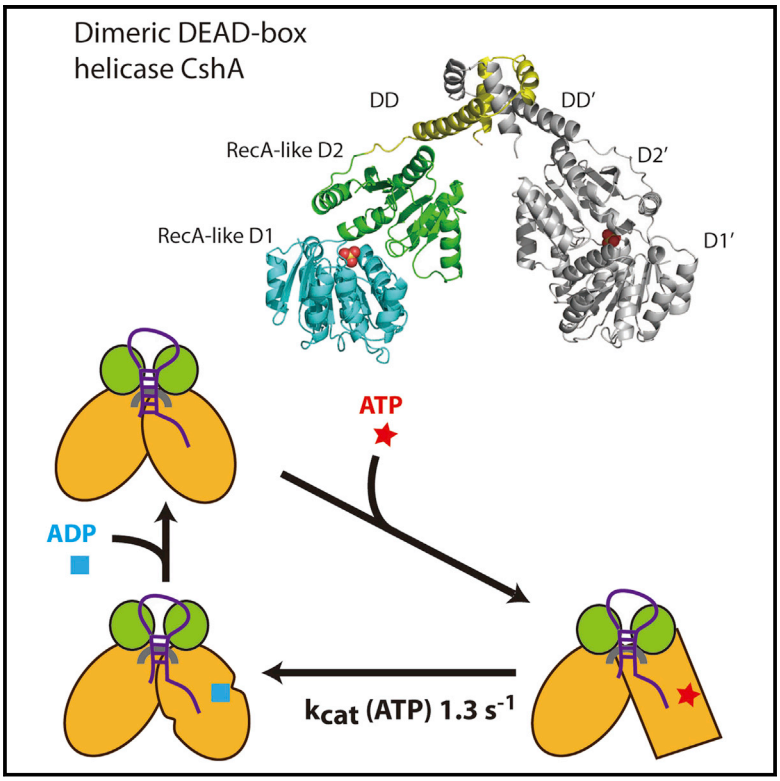

Authors

Jennifer Huen, Chia-Liang Lin, Bagher Golzarroshan, Wan-Li Yi, Wei-Zen Yang, Hanna S. Yuan

Correspondence

hanna@sinica.edu.tw

In Brief

Huen et al. report the crystal structure of CshA, a unique dimeric DEAD-box helicase. CshA binds RNA with or without ATP/ADP, as RNA remain bound with CshA during ATP hydrolysis cycles. RNA is thus degraded processively through cooperation between exoribonucleases and CshA in the RNA-degrading machinery.

Highlights

- CshA is a unique dimeric DEAD-box helicase in the RNA degradosome for RNA decay
- The crystal and SAXS structures of CshA reveal a flexible V-shaped structure
- Dimerization of CshA produces a helicase that binds RNA with or without ATP
- Dimeric CshA cooperates with exoribonucleases to unwind and degrade RNA

Accession Numbers

5IVL

Huen et al., 2017, Structure *25*, 469–481
March 7, 2017
http://dx.doi.org/10.1016/j.str.2017.01.012

Structure
Article

Structural Insights into a Unique Dimeric DEAD-Box Helicase CshA that Promotes RNA Decay

Jennifer Huen,[1] Chia-Liang Lin,[1] Bagher Golzarroshan,[1,2,3] Wan-Li Yi,[1] Wei-Zen Yang,[1] and Hanna S. Yuan[1,4,5,*]
[1]Institute of Molecular Biology
[2]Chemical Biology and Molecular Biophysics Program, Taiwan International Graduate Program
Academia Sinica, Taipei, Taiwan 11529, ROC
[3]Institute of Bioinformatics and Structural Biology, National Tsing Hua University, Hsinchu, Taiwan 30013, ROC
[4]Graduate Institute of Biochemistry and Molecular Biology, National Taiwan University, Taipei, Taiwan 10048, ROC
[5]Lead Contact
*Correspondence: hanna@sinica.edu.tw
http://dx.doi.org/10.1016/j.str.2017.01.012

SUMMARY

CshA is a dimeric DEAD-box helicase that cooperates with ribonucleases for mRNA turnover. The molecular mechanism for how a dimeric DEAD-box helicase aids in RNA decay remains unknown. Here, we report the crystal structure and small-angle X-ray scattering solution structure of the CshA from *Geobacillus stearothermophilus*. In contrast to typical monomeric DEAD-box helicases, CshA is exclusively a dimeric protein with the RecA-like domains of each protomer forming a V-shaped structure. We show that the C-terminal domains protruding outward from the tip of the V-shaped structure is critical for mediating strong RNA binding and is crucial for efficient RNA-dependent ATP hydrolysis. We also show that RNA remains bound with CshA during ATP hydrolysis cycles and thus bulk RNAs could be unwound and degraded in a processive manner through cooperation between exoribonucleases and CshA. A dimeric helicase is hence preserved in RNA-degrading machinery for efficient RNA turnover in prokaryotes and eukaryotes.

INTRODUCTION

The DEAD-box proteins are the largest family of RNA helicases involved in almost every aspect associated with gene expression, such as transcription, translation, mRNA splicing, and RNA turnover (Jarmoskaite and Russell, 2014). DEAD-box proteins are ATP-dependent enzymes that couple ATP hydrolysis with RNA remodeling, and they all contain the conserved RecA-like 1 (D1) and RecA-like 2 (D2) helicase core domains that consist of 12 characteristic sequence motifs essential for ATP binding, ATP hydrolysis, RNA binding, and RNA remodeling (Linder and Jankowsky, 2011). Binding of ATP at the catalytic site formed between D1 and D2 domains typically enhances RNA binding of the DEAD-box proteins (Russell et al., 2013). Accessory domains at the N or C terminus usually participate in RNA interactions or protein-protein interactions, lending specificity to the DEAD-box proteins for their defined roles in vivo (Rudolph and Klostermeier, 2015).

Most of the DEAD-box proteins function as monomeric enzymes with a single D1/D2 helicase core, catalyzing the unwinding of short RNA duplexes by local strand separation (Linder and Fuller-Pace, 2013). The crystal structures of monomeric DEAD-box helicases, such as eIF4A (Andersen et al., 2006), Mss116p (Mallam et al., 2012), and Vasa (Sengoku et al., 2006), reveal that binding of RNA and ATP triggers a closed conformational change of the D1/D2 helicase core that facilitates extrusion of the annealed RNA strand by the "wedge" helix in D1 (Ozgur et al., 2015). After RNA remodeling, ATP hydrolysis induces the release of the second RNA strand and re-opening of the helicase core (Henn et al., 2012). Thus, the monomeric DEAD-box helicases are weak processive enzymes, unwinding RNA less than two turns and dissociating from RNA after ATP hydrolysis (Russell et al., 2013).

In contrast, only a handful of DEAD-box helicases are homodimeric enzymes, including RNA helicase B (RhlB), heat-resistant RNA-binding ATPase (Hera), and cold shock helicase A (CshA) (Giraud et al., 2015; Lehnik-Habrink et al., 2010; Liou et al., 2002; Rudolph and Klostermeier, 2009). RhlB and CshA are components of the bacterial RNA degradosome, which participates in RNA degradation and is important in regulating specific transcripts in response to cellular environments (Eidem et al., 2012; Górna et al., 2012; Laalami et al., 2014; Lehnik-Habrink et al., 2012; Rorbach and Minczuk, 2012; Szczesny et al., 2012). In Gram-negative bacteria, such as *Escherichia coli*, the RNA degradosome complex is composed of the endoribonuclease RNase E (Carpousis et al., 1994), the exoribonuclease PNPase (polynucleotide phosphorylase) (Carpousis et al., 1994; Mohanty and Kushner, 2000), the glycolytic enzyme enolase (Commichau et al., 2009; Py et al., 1996), and the helicase RhlB (Lin and Lin-Chao, 2005; Py et al., 1996). Structured RNA substrates are unwound by the ATP-dependent RhlB helicase, and its interaction with PNPase and RNase E allows rapid RNA degradation by the endo- and exoribonucleases (Chandran et al., 2007; Coburn et al., 1999; Liou et al., 2002). PNPase is a 3′ to 5′ exoribonuclease that removes single nucleotides processively from the 3′ end of an RNA chain (Fazala et al., 2015). PNPase only digests single-stranded RNA (ssRNA) due to its narrow RNA-binding channel located in the center of a ring-like trimeric structure (Hardwick et al., 2012; Lin et al., 2012; Shi

et al., 2008; Symmons et al., 2000). During digestion of structured RNA, the exoribonuclease activity of PNPase is promoted by RhlB helicase (Lin and Lin-Chao, 2005; Liou et al., 2002). PNPase forms a 3:2 complex (~365 kDa) with RhlB helicase and this so-called "minimal RNA degradosome" contributes to *cysB* mRNA degradation under oxidative stress (Lin and Lin-Chao, 2005; Tseng et al., 2015). In human mitochondria, a similar protein complex, named the mitochondrial exosome, consisting of a dimeric Suv3 helicase and PNPase, was characterized (Borowski et al., 2013; Wang et al., 2009). Therefore, a dimeric helicase, which cooperates with PNPase, is preserved in the minimal RNA degradosome and mitochondrial exosome for RNA decay in prokaryotes and eukaryotes.

The DEAD-box helicase CshA shares 39% sequence identity with RhlB and is likely the functional homolog of RhlB in the RNA degradosome of Gram-positive bacteria lacking RNase E (Ando and Nakamura, 2006; Lehnik-Habrink et al., 2010; Pandiani et al., 2011). In *Bacillus subtilis*, the RNA degradosome-like complex is composed of RNase Y, PNPase, RNase J1, RNase J2, enolase, phosphofructokinase (PfkA), and CshA, as assessed by a combination of affinity co-purification and two-hybrid approaches (Commichau et al., 2009; Lehnik-Habrink et al., 2010). A similar RNA degradosome complex has also been identified in *Staphylococcus aureus* that contains an additional component of the RNase RnpA (Roux et al., 2011). CshA is important for the cold shock response in *B. subtilis* and quorum sensing regulation in *S. aureus* (Oun et al., 2013). Bacterial two-hybrid analyses have shown that CshA of *B. subtilis* interacts with the PNPase, enolase, and PfkA components of the RNA degradosome, whereas CshA of *S. aureus* interacts with enolase, PfkA, RnpA, and RNase Y (Lehnik-Habrink et al., 2010; Roux et al., 2011). Co-expression of *S. aureus* CshA and RNase J1 in *E. coli* showed that CshA and RNase J1 are co-purified, suggesting that CshA and RNase J1 directly interact (Giraud et al., 2015). Collectively, these results suggest that CshA helicase plays a central role in the RNA degradosome, cooperating with various endo- and exoribonucleases for efficient RNA turnover.

Despite these advances, our understanding in the molecular mechanism of how a DEAD-box helicase functions with the exoribonuclease PNPase in the minimal RNA degradosome to promote RNA decay is limited. Here, using CshA from *Geobacillus stearothermophilus* as a model DEAD-box helicase, we examine how a dimeric DEAD-box helicase cooperates with PNPase for RNA unwinding and degradation. CshA contains two additional C-terminal accessory domains besides the two canonical RecA-like D1 and D2 domains: a dimerization domain (DD) and a C-terminal domain (CTD) (Figure 1A). The DD in CshA shares about 33% sequence identity with that of Hera and is responsible for helicase dimerization (Klostermeier and Rudolph, 2009; Steimer et al., 2013). On the other hand, the CTD (46 amino acids, 422–467) shares low sequence identity with the RNA-binding module in Hera (8%, 87 amino acids) and YxiN (6%, 76 amino acids). The CTD of CshA from *S. aureus* is required for degradation of bulk mRNA and for interaction with components of the RNA degradosome (Giraud et al., 2015). Here, we report the crystal structure of CTD-truncated CshA (residues 1–421) from *G. stearothermophilus* at a resolution of 2.3 Å. We demonstrate how CshA forms a dimer and, via CTD, can remain bound to RNA as the helicase core hydrolyzes ATP. Taken together, we suggest that, while CshA works with PNPase, structured RNA remain tethered to the CshA-PNPase complex and thus can be degraded efficiently in a processive manner.

RESULTS

CshA Forms Homodimers to Unwind Duplex RNA with or without Overhangs

To gain a better understanding of how each domain of CshA functions in RNA decay, we first constructed the expression vectors for the full-length CshA (residues 1–467) from *G. stearothermophilus* and two CshA truncation mutants, CshA-ΔCTD (CTD-truncated CshA, residues 1–421) and CshA-ΔDD/CTD (DD- and CTD-truncated CshA, residues 1–359) (Figure 1A). These three C-terminal His-tagged CshA proteins were overexpressed in *E. coli* and purified by chromatographic methods to a high homogeneity as revealed by SDS-PAGE (Figure 1B, left panel). After addition of the crosslinker EDC to the recombinant proteins, CshA and CshA-ΔCTD migrated as dimers, whereas CshA-ΔDD/CTD migrated as monomers in the SDS-PAGE after EDC crosslinking (Figure 1B, right panel), suggesting that DD is responsible for dimer formation.

To corroborate this result, the three recombinant proteins were eluted respectively by size-exclusion chromatography and their molecular weights were measured by multi-angle light scattering: 109.9 kDa for CshA (calculated mass, 53.5 kDa), 99.1 kDa for CshA-ΔCTD (calculated mass, 48.3 kDa) and 43.1 kDa for CshA-ΔDD/CTD (calculated mass, 41.3 kDa) (Figure 1C). These results confirm that CshA and CshA-ΔCTD form homodimers, whereas CshA-ΔDD/CTD forms monomers in solutions, and therefore, DD is responsible for CshA dimerization. Moreover, CshA and CshA-ΔCTD had a thermal melting temperature (T_m) of 68°C as determined by circular dichroism (Figure S1A). In contrast, CshA-ΔDD/CTD had a T_m of 60°C, indicating that the DD contributed not only to protein dimerization but also to protein stability. In summary, these results confirm that full-length CshA forms a stable homodimer via the DD.

We next asked if CshA from *G. stearothermophilus* unwinds duplex RNA. We incubated CshA with a Cyanine-3-labeled duplex RNA (11 base pairs) with or without an 11-nucleotide (nt) overhang at 5′ or 3′ end (see the schematic diagram in Figure 1D). With increased concentrations of CshA, all the three types of the duplex RNA were gradually unwound in the presence of ATP (see the native PAGE in Figure 1D). The duplex RNA with a 5′ or 3′ overhang were unwound more efficiently than the blunt-end duplex RNA, suggesting CshA prefers to unwind duplex RNA with an overhang. Moreover, in the absence of ATP, the duplex RNA could not be unwound by CshA. Taken together these results demonstrate that our purified recombinant CshA actively unwinds duplex RNA with or without overhangs in an ATP-dependent manner.

C-Terminal Domain of CshA Is Responsible for Strong RNA Binding

The N- or C-terminal accessory domains of DEAD-box proteins are commonly involved in RNA binding or protein-protein interactions (Hardin et al., 2010; Karow and Klostermeier, 2010; Mallam et al., 2011; Rudolph and Klostermeier, 2009). To investigate the functional importance of the CTD and DD, we tested the

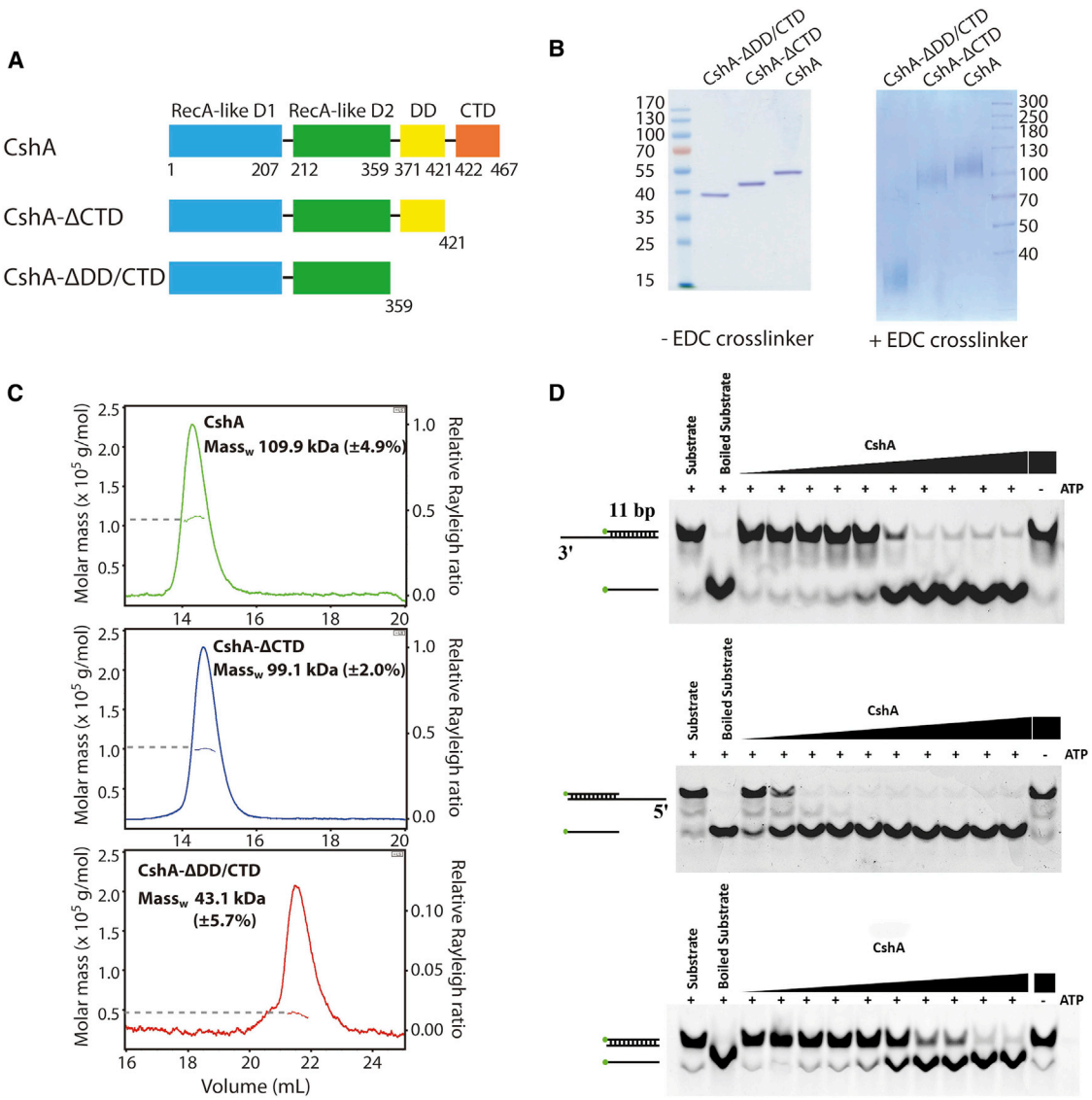

Figure 1. CshA Forms a Homodimer and Unwind Duplex RNA in an ATP-Dependent Manner

(A) Illustration of CshA protein constructs used in this study: CshA, CshA-ΔCTD, and CshA-ΔDD/CTD.

(B) SDS-PAGE of the purified CshA proteins in non-crosslinked (left) and EDC-crosslinked (right) conditions.

(C) Samples of CshA, CshA-ΔCTD, and CshA-ΔDD/CTD were applied to a SEC detector coupled to a MALS detector and represented as elution profiles.

(D) The RNA unwinding activity of CshA is shown on native PAGE with a starting CshA concentration of 60 μM and a serial 5-fold dilution. A 5′ end Cyanine-3-labeled RNA (11 nucleotides) was annealed with an 11- or 22-nt RNA to prepare a duplex RNA (11 base pairs) with or without an 11-nt overhang at the 5′ or 3′ end. CshA had no unwinding activity in the absence of ATP.

ability of CshA truncation mutants to bind RNA. We used three different 5′-end Cy3-labeled RNA substrates: a blunt-ended stem-loop RNAs with 8 base pairs in the stem region (referred to as SL), a single-stranded 20-nt poly(A) RNA (A20), and a stem-loop RNA with a 10-nt 3′ poly(A) overhang (SL-A10). These RNA substrates were incubated with the recombinant CshA proteins, and the fluorescence polarization signals were measured to monitor RNA-protein interactions (Figure 2A). It should be noted that the K_d values were calculated based on the assumption that one substrate is bound to one monomeric CshA proteins, in a simple bimolecular binding reaction. Based on our stoichiometric binding results (see below), the binding mode of small ssRNA is different than that of stem-loop RNAs as ssRNA can bind a CshA dimer at two sites indicating that the two K_d values cannot be compared directly. Full-length CshA had the highest RNA-binding affinity, with an apparent K_d of 0.20 μM for SL RNA, an 65- and 30-fold greater RNA-binding activity compared with CshA-ΔCTD (K_d = 13.68 μM) and CshA-ΔDD/CTD (K_d = 5.87 μM), respectively.

For the SL RNA, CTD alone exhibited a K_d of 0.86 μM, which is about 15- and 7-fold stronger binding than for CshA-ΔCTD and CshA-ΔDD/CTD, respectively. These results indicate that RNA binding by CshA is predominantly mediated by CTD. In addition, CTD showed slightly better binding to the A20 and SL-A10

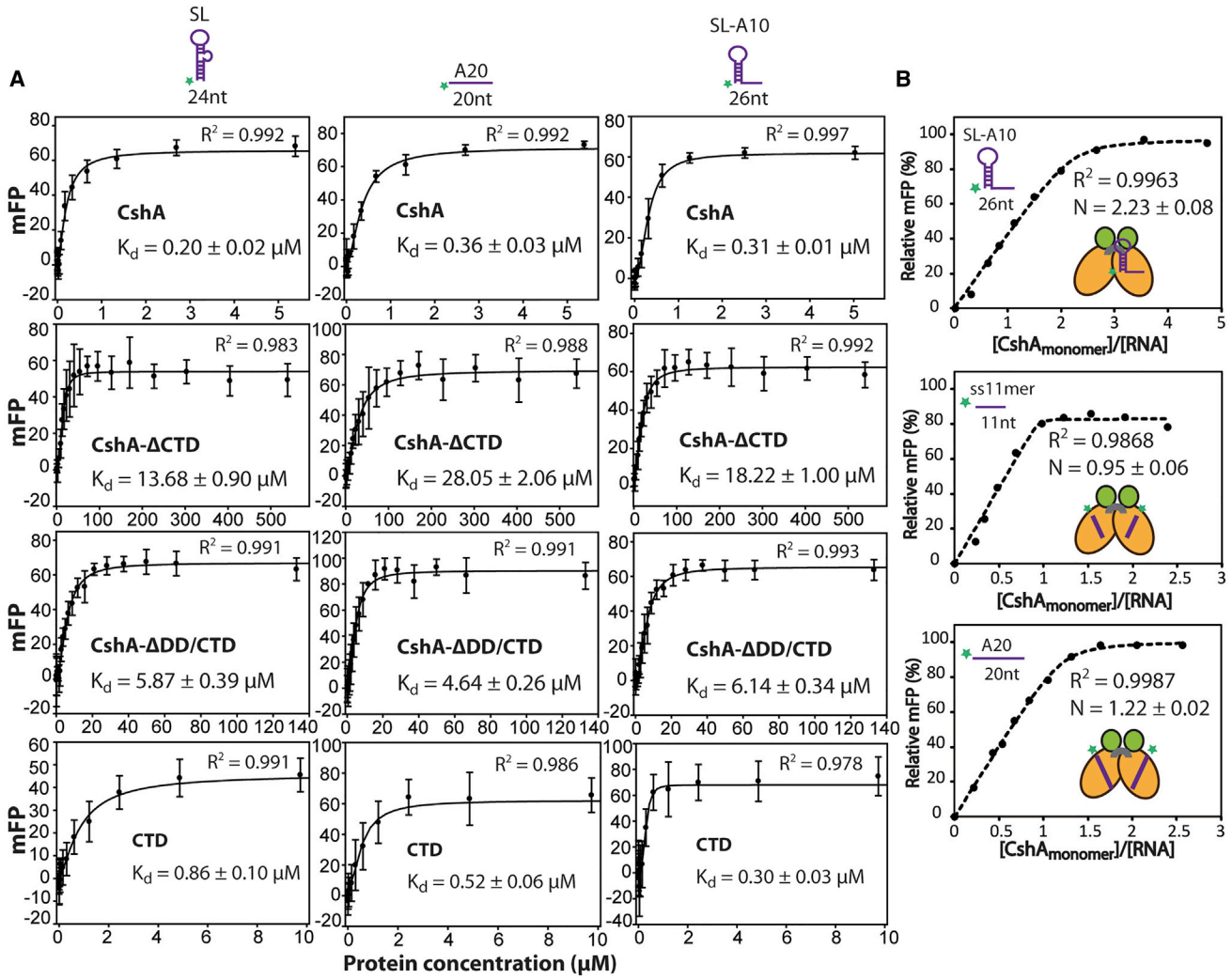

Figure 2. CshA Binds RNA Strongly Via Its C-Terminal Domain

RNA binding as measured by fluorescence polarization (in mFP units) is plotted against protein concentration.

(A) The RNA substrates used are illustrated at the top: SL, A20, and SL-10. The average of three independent experiments is shown with error bars representing one SD. K_d values with SEs were obtained by fitting the equation in the Experimental Procedures. The green stars mark the Cy3-labeled position at the 5′ end of the RNA substrate.

(B) Stoichiometric RNA binding by FP assays using SL-A10, ss11mer, and A20 RNA substrates. Stoichiometric equivalence point (N) was determined as described in the Experimental Procedures. A schematic of CshA is shown where the orange oval represents the D1 and D2 domains and the green circle represents the CTD. See also Figure S1.

RNAs, both of which contained free-end single-stranded regions, in comparison with the blunt-ended SL RNA, suggesting that the CTD may prefer binding ssRNA. Full-length CshA exhibits strongest binding to stem-loop RNAs (K_d = 0.20–0.31 μM) compared with CTD alone (K_d = 0.30–0.86 μM) and CshA-ΔCTD (K_d = 13.68–18.22 μM), indicating that the CTD and D1/D2 core work together to stabilize binding to stem-loop RNAs.

CshA Dimer Binds One Stem-Loop RNA

RNA binding by DEAD-box proteins requires a specific orientation of the 5′ and 3′ ends; the D2 domain binds at the 5′-end and the D1 domain at the 3′-end (Collins et al., 2009; Del Campo and Lambowitz, 2009; Mallam et al., 2014; Ozgur et al., 2015; Sengoku et al., 2006; von Moeller et al., 2009; Xiol et al., 2014). It is intriguing how a structured RNA, such as a stem-loop RNA, is bound to the dimeric CshA, either with a one-to-two or two-to-two ratio between RNA and protein. To assess the stoichiometry of RNA binding by CshA, we performed fluorescence polarization assays at stoichiometric binding concentrations (~25 × K_d, Figure 2B). The stoichiometric equivalence point (N) was determined by fitting the data to the quadratic equation in the Experimental Procedures.

For binding of the single-stranded 11-nt RNA, we observed an equivalence point (N) of 0.95, suggesting that two small RNAs could bind the CshA dimer simultaneously (Figure 2B). A schematic diagram of CshA (orange ovals represent RecA-like helicase cores, gray loop represents DD, and green circles

Table 1. X-Ray Diffraction and Refinement Statistics for CshA-ΔCTD

Data Collection Statistics	
Space group	$P2_1$
Cell dimensions	
a, b, c (Å)	58.49, 96.31, 83.77
β (°)	95.21
Wavelength (Å)	1.0
Resolution (Å)	30.0–2.3 (2.38–2.30)[a]
Observed reflections	307,783
Unique reflections	40,920
Completeness (%)	99.7 (100.0)
<I>/<σI>	32.84 (4.42)
R_{merge} (%)	6.1 (31.9)
Refinement Statistics	
Resolution range (Å)	23.52–2.30
Reflections (working/test)	38,844/2,057
R_{work}/R_{free} (%)	20.22/25.07
No. of atoms (protein/water)	6,476/210
Average B factor (Å^2)	46.0
RMSD (bond length [Å]/bond angle [°])	0.002/0.651
Ramachandran favored regions (%)	100
Ramachandran outliers (%)	0

RMSD, root-mean-square deviation.
[a]Highest-resolution shell is shown in parentheses.

represent CTDs) and RNA (purple) is shown in the inset to illustrate binding stoichiometry and does not represent the mode of binding. In the presence of the longer single-stranded A20 RNA substrate, N was 1.22, suggesting one CshA dimer still bound two long ssRNA. In contrast, using the stem-loop RNA (SL-A10) as the substrate, we observed an equivalence point (N) of 2.23, suggesting that one CshA dimer bound one stem-loop RNA (Figure 2B). These results suggest that CshA dimer potentially could bind two ssRNAs, whereas in the presence of folded structured RNA, CshA could only accommodate one of those substrates. Binding of one structured RNA by the dimeric CshA indicates that CshA unwinds duplex RNA one substrate at a time rather than each protomer unwinding its own substrate. Thus, together with our helicase assay data, we demonstrate that a dimeric DEAD-box helicase binds and unwinds one structured RNA substrate.

Crystal Structure of CshA-ΔCTD

To reveal the molecular assembly of CshA, we screened the crystallization conditions for the three proteins and crystallized only CshA-ΔCTD in the monoclinic $P2_1$ unit cell with one dimer per asymmetric unit by the hanging-drop vapor diffusion method. The crystal structure of CshA-ΔCTD was determined by molecular replacement using the crystal structure of *B. subtilis* YxiN as the search model (PDB: 2HJV) (Caruthers et al., 2006). After location of the two RecA-like D1/D2 domains in the CshA dimer, the DD was manually built based on the extra electron density in the Fourier maps. Three loops (A207-V212, A334-T337, and N394-S396) had ill-defined electron density and were omitted during refinement. The final crystal structure of CshA was refined up to a resolution of 2.3 Å. The diffraction and final refinement statistics are listed in Table 1.

CshA-ΔCTD forms a V-shaped dimeric structure with each protomer bound to a SO_4^{2-} ion in the ATP-binding pocket at the interface between the RecA-like D1 and D2 domains (Figure 3A). Dimerization of the two protomers is mediated by the DD containing three α helices (α17-α19). Dimerization involves all three α helices, where small non-polar residues make extensive hydrophobic contacts with neighboring residues (see Figure 3B). The inner face of the α17 helix containing L386, L387, V389, and V390 forms a hydrophobic patch with the small aliphatic residues of the α18′ and α19′ helices of the other protomer (Figure 3C). The crystal structure of a truncated Hera containing DD and one of the RecA-like domains (D2 domain only) (PDB: 3I32) have been reported (Klostermeier and Rudolph, 2009). We superimposed DD of CshA with that of the truncated Hera showing that the DDs of the two proteins share similar secondary structures of three α helices but they have different orientations, giving an average root-mean-square deviation (RMSD) of 2.9 Å for 51 Cα atoms (Figure 3D). The differences in their orientations suggest the conformation flexibility of the DD resulting in V-shaped arms that open more than 20° in CshA than that of the Hera (Figure 3D).

The unique DD of CshA brings together two D1/D2 helicase cores located in two arms of the V-shaped structure. The arms of the dimeric "V" are each composed of D1/D2 RecA-like domains and, in both arms, D1 and D2 appear in an "open" conformation. However, this is unlike the open conformation of DEAD-box proteins observed in the apo-, ADP-, or SO_4^{2-}-bound forms, for which D1 and D2 show variable orientations and distances from each other with no identifiable contacts between domains (Collins et al., 2009; Hogbom et al., 2007; Klostermeier, 2013; Ozgur et al., 2015; Story et al., 2001). The CshA structure neither resembles the catalytically active closed conformation (Collins et al., 2009; Del Campo and Lambowitz, 2009; Mallam et al., 2012, 2014; Sengoku et al., 2006; von Moeller et al., 2009; Xiol et al., 2014). Structural alignment of D1 domains of CshA and Mss116 (PDB: 3I5X) gives an RMSD of 0.8 Å over 115 Cα atoms. With respect to the aligned D1 domains, the entire D2 domain of CshA is rotated about 30° from the position of D2 of Mss116 in the closed conformation (Figure 3E).

Several observations highlight some unique features of the CshA structure not seen in other DEAD-box proteins. First, in the structure of Mss116 bound to AMP-PNP and ssRNA, the RNA-binding surface formed by motifs Ia-c in D1 and motifs IV and V in D2 follows the curve of the bound ssRNA (Figure 3E) (Del Campo and Lambowitz, 2009). The "wedge" α helix formed by motif Ic in D1 kinks the ssRNA and is the driving force for displacing one strand of a duplex RNA substrate, resulting in a closed conformation of the RecA-like core domains (Del Campo and Lambowitz, 2009; Sengoku et al., 2006). In contrast, motif V of D2 in the CshA structure is bent toward the central axis of the dimer such that the RNA-binding surface between D1 and D2 is rotated significantly and would require several sharp bends in RNA if one was to be bound. This rotation of the RNA-binding region would likely decrease its affinity for RNA, hinting that the structure of CshA is not in the catalytically active state. Secondly, several key residues that are important for ATP binding and

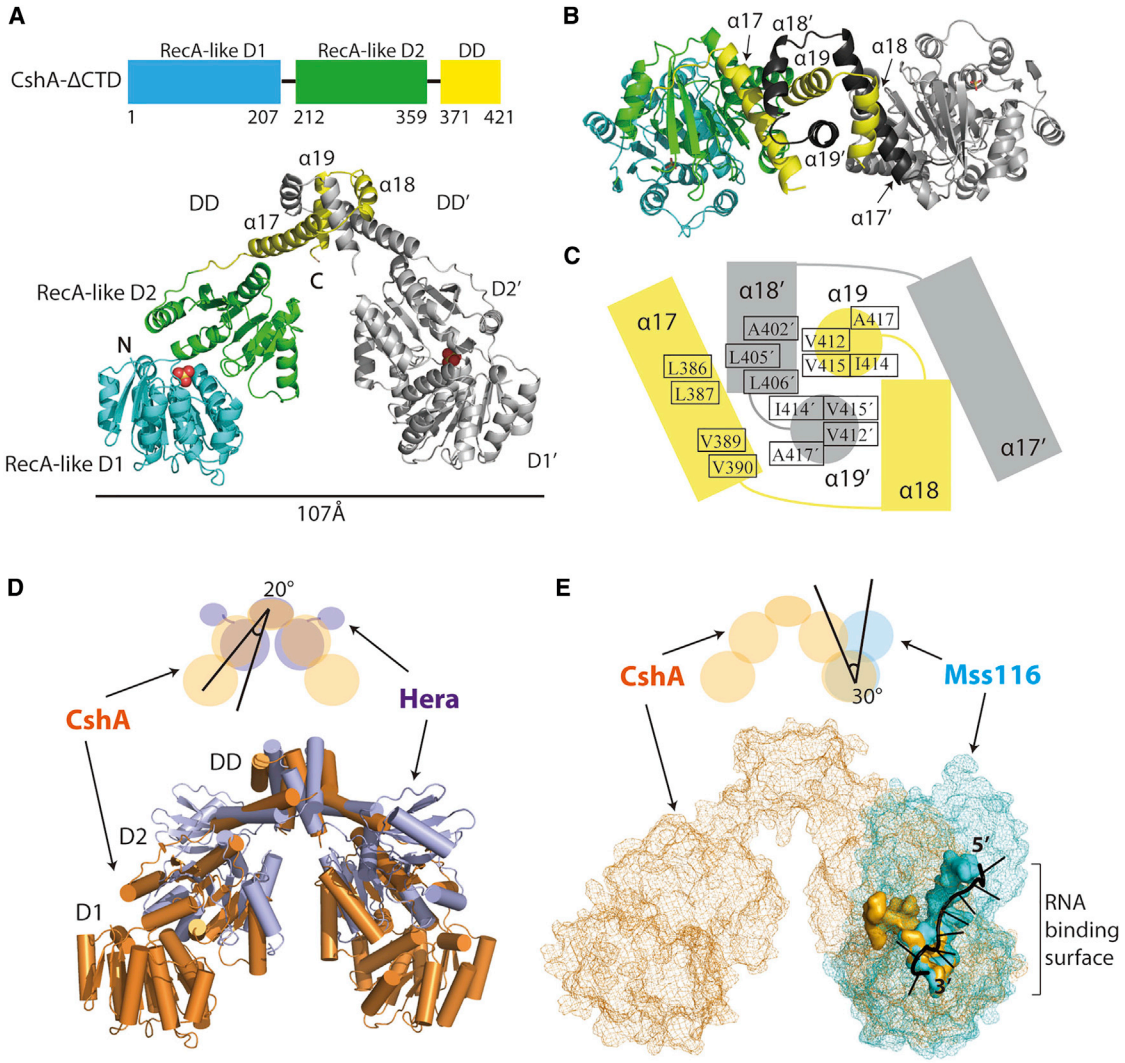

Figure 3. Crystal Structure of CTD-Truncated CshA Reveals a Homodimeric V-Shaped Structure

(A) Crystal structure of dimeric CshA-ΔCTD with the left protomer colored by domain. The three α helices involved in dimerization are labeled α17-α19 for the left protomer and α17′-α19′ for the right protomer.

(B and C) Illustration of the aliphatic residues of the α17-α19 and α17′-α19′ helices involved in dimerization.

(D) Superposition of the DD domain of CshA (orange) on the DD domain of Hera (purple, PDB: 3I32). The protomer arms of CshA are rotated 20° outward from the D2 position of Hera resulting in a wider V-shaped conformation.

(E) Superposition of the RecA-like D1 domain of CshA-ΔCTD (orange) on the D1 domain of Mss116 (cyan, PDB: 3I5X) bound to polyU-10 single-stranded RNA (black). A ~30° rotation is observed for D2 of CshA relative to D2 of Mss116 (top panel). The RNA binding region of Mss116 and the equivalent region in CshA are shown as cyan and orange surfaces, respectively. See also Figure S2.

hydrolysis are collapsed or shifted away from the ATPase site in comparison with the ATP-bound conformation (Figures S2A and S2B). The phosphate-binding loop, which in the active state is normally in the open conformation to accommodate the Mg^{2+} and γ-phosphate of ATP (Figures S2C and S2D) (Del Campo and Lambowitz, 2009; Sengoku et al., 2006; von Moeller et al., 2009; Xiol et al., 2014), is more collapsed in CshA (Figure S2E).

Moreover, a structural model of CshA dimer bound with two duplex RNA was constructed using the crystal structure of Mss116 RecA-like D2 domain bound with a duplex RNA (Mallam et al., 2012) as a template (see Figure S3A). The two duplex RNAs bound with CshA are clashed in the model, suggesting that CshA dimer binds only one duplex RNA due to steric hindrance. This result is consistent with the RNA-binding assay showing that CshA dimer binds only one stem-loop RNA (Figure 2B). In summary, our CshA structure reveals a unique V-shaped structure of a dimeric DEAD-box helicase with complete RecA-like D1/D2 cores and a SO_4^{2-}-bound inactive conformation for the helicase core domains.

SAXS Reveals the Location of CTD and a Flexible Extended Conformation of CshA

To determine the location of the CTD and the conformation of CshA in solution, we conducted small-angle X-ray scattering

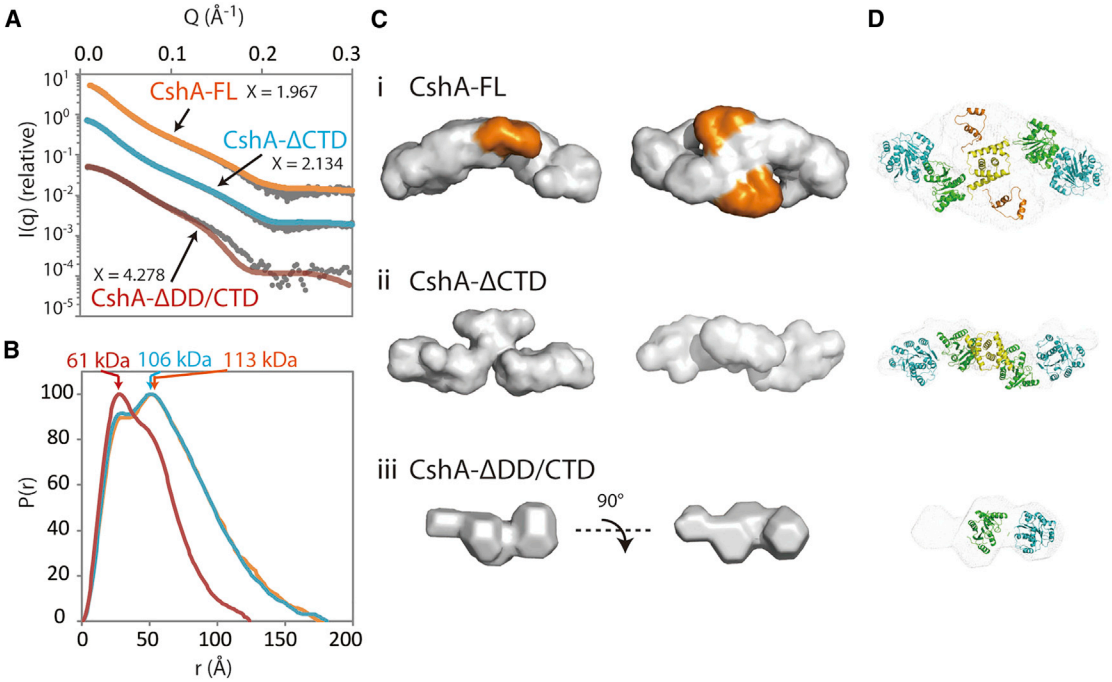

Figure 4. Solution SAXS Structure of CshA Reveals that the CTD Extends Outward from the Dimerization Domain

(A) Small-angle X-ray scattering (SAXS) curves are represented as logarithmic scattering intensities. Theoretical scattering intensities generated for envelopes, shown in (C), are fitted to experimental data and are colored orange for CshA ($\chi = 1.967$), blue for CshA-ΔCTD ($\chi = 2.134$), and red for CshA-ΔDD/CTD ($\chi = 4.278$).

(B) Distance distribution functions are shown in the same color scheme as in (A). Radii of gyration are labeled above the curve peaks and maximum diameters at the curve peak tails.

(C) Envelopes of CshA (top panel), CshA-ΔCTD (middle panel), and CshA-ΔDD/CTD (bottom panel) were determined by GASBOR and DAMMIN. The orange region in the CshA envelope represents a density corresponding to the CTD not present in CshA-ΔCTD. (D) Rigid domains using the CshA-ΔCTD crystal structure and homology model of CTD (modeled with PDB: 2KKE) were fitted into the envelopes in (C). CshA and CshA-ΔCTD exhibit extended V shapes, while the CshA-ΔDD/CTD monomer shows a bi-lobed structure. See also Figures S3 and S4.

(SAXS) experiments (Figure 4A). For all constructs, the distance distribution functions show characteristic smoothing toward 0 as r approaches D_{max} (Figure 4B), suggesting flexibility. The molecular mass values estimated by SAXS (Figure 4C) are in agreement with the weighted mass values of each construct as estimated by multi-angle light scattering (Figure 1C). For CshA and CshA-ΔCTD, the P(r) functions show a larger distance distribution with peak maxima around 50 Å as expected for the dimeric forms.

Ab initio modeling methods, DAMMIN and GASBOR, were used for shape determination of all constructs (Petoukhov et al., 2012). Envelope structures of both CshA and CshA-ΔCTD show a splayed V-shape with extended arms of D1/D2 helicase core domains. An additional density present in the envelope of CshA (orange, Figure 3C), but not CshA-ΔCTD, indicates the location of the CTD, which extends out from the DDs. A structural homology search of the CTD identified a small dimeric methanobacterial protein of unknown function (PDB: 2KKE) containing a helix-loop-helix motif (Figure S3A), and a homology model of the CTD to this protein was generated containing mainly two α helices (Figure S3B). We further expressed and purified CTD (Figure S3C), and confirmed that CTD contains α-helical structures as revealed by the CD spectrum (Figure S3B). This α-helical CTD model was easily fit into the additional density in our SAXS structure (orange region in Figure 4C), suggesting a splayed V-shaped structure for the full-length CshA (Figure 4D).

To test the flexibility of CshA, we further calculated the dimensionless Kratky and Porod-Debye plots revealing that all constructs exhibit some degree of flexibility (Bernado, 2010; Rambo and Tainer, 2011) (Figures S4A and S4B). This result propelled us to further model CshA by the ensemble optimization method (Petoukhov et al., 2012). Seven major CshA conformers were generated and the ensemble gave comparable fitting curves with the experimental SAXS data as the envelope model (Figures S4C and S4D). Several conformers exhibited V shapes similar to the crystal structure of CshA, suggesting that the crystal structure likely represents one of the conformations of this flexible helicase (Figure S4E). Thus, our SAXS analyses demonstrate that CshA exhibits a flexible V-shaped structure with CTD protruding outward from the DD in the apex region.

RNA Binding by the CshA Is Independent of ATP

DEAD-box helicases utilize ATP binding and hydrolysis for RNA remodeling, so we next tested how RNA binding was affected in the presence of ATP and ADP. Typically, DEAD-box proteins exhibit some degree of nucleotide-dependent RNA binding and, in some cases, as with mouse eIF4A, yeast Ded1 and YxiN of *B. subtilis*, they do not bind RNA without the presence of ATP (Iost et al., 1999; Lorsch and Herschlag, 1998; Samatanga

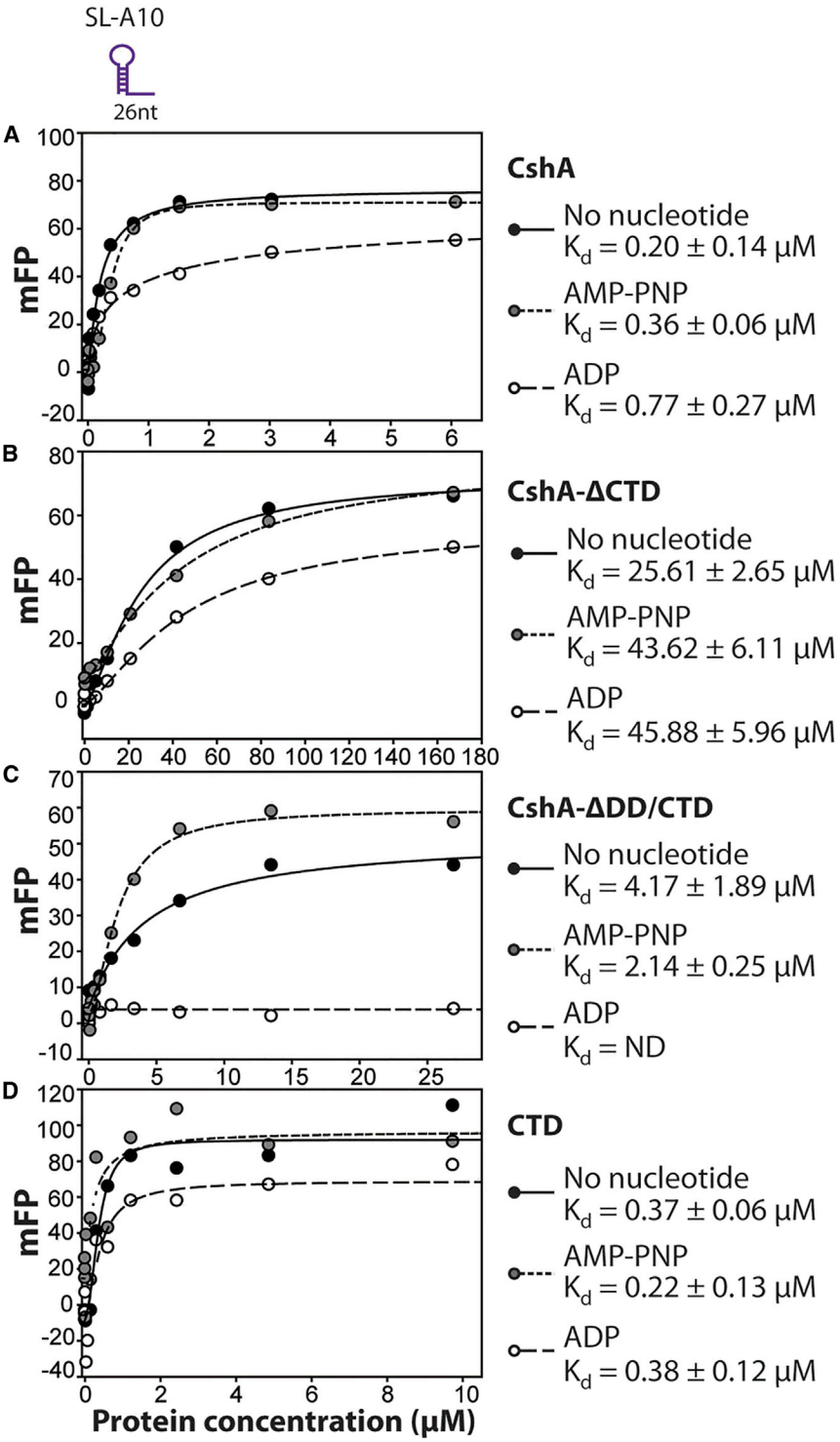

Figure 5. CshA Binds RNA in an ATP-Independent Manner

RNA binding as measured by fluorescence polarization in the absence and presence of 1 mM AMP-PNP or ADP. Data are shown for (A) CshA, (B) CshA-ΔCTD, (C) CshA-ΔDD/CTD, and (D) the CTD domain in the presence of ADP (hollow circles, long dash line), in the presence of AMP-PNP (gray circles, short dashed line), or in the absence of nucleotide (black circles, solid line). K_d values with SE of fitting are shown on the right. See also Figures S5 and S6.

and Klostermeier, 2014). RNA-binding assays were conducted as described above, but in the presence of 1 mM of the ATP analog AMP-PNP or ADP. Unexpectedly, in the presence or absence of AMP-PNP, CshA exhibited apparent K_d values of 0.20 and 0.36 μM for binding of the stem-loop RNA (SL-A10), respectively, showing that CshA binds RNA tightly with or without the presence of ATP (Figure 5A). A similar result was observed for CshA of *B. subtilis* (Ando and Nakamura, 2006). However, in the presence of ADP, CshA bound RNA with a K_d of 0.77 μM, suggesting that ATP hydrolysis and accumulation of ADP reduces the RNA-binding affinity of CshA. Indeed, the time course of fluorescence polarization revealed that RNA binding was reduced over time in the presence of ATP and ADP, but not AMP-PNP (Figure S5). CshA-ΔCTD bound RNA with a lower affinity overall and affinity reduced in the presence of AMP-PNP or ADP (K_d = ~45 μM) (Figure 5B).

As expected, RNA binding by the CTD alone does not appear to be affected by ATP or ADP (Figure 5D). Nucleotide-independent binding by the CTD would allow RNA to remain tethered to CshA as the D1/D2 catalytic core cycles through RNA binding and release during ATP hydrolysis. In contrast, CshA-ΔDD/CTD bound RNA in a nucleotide-dependent manner, as it bound RNA with a highest affinity in the presence of AMP-PNP (K_d = 2.14 μM), but had no detectable binding in the presence of ADP (Figure 5C). In this regard, the CshA-ΔDD/CTD mutant more closely assumes the ATP/ADP-dependent RNA-binding characteristics of other monomeric DEAD-box proteins (such as YxiN and Mss116), and indicates that the ancestral function of the core RecA-like domains is highly conserved. Our binding results indicate that dimerization of two D1/D2 cores allows RNA to remain bound in the presence of ADP, whereas in the case of a single D1/D2 core, RNA binding is abrogated. The presence of the CTDs ensures that RNA remains bound while the D1/D2 core cycles through ATP hydrolysis and RNA unwinding during RNA decay.

RNA Binding at the C-Terminal Domain Enhances ATP Hydrolysis

The ATPase activity of DEAD-box proteins is typically enhanced upon binding to an RNA substrate (Ando and Nakamura, 2006;

Table 2. The ATP Hydrolysis Catalytic Parameters of CshA with or without the Presence of RNA

		K_m (mM)	k_{cat} (s^{-1})
CshA	–	0.78 ± 0.07	0.09 ± 0.02[b]
	+RNA[a]	0.16 ± 0.01	1.28 ± 0.11[b]
CshA-ΔCTD	–	ND	ND
	+RNA	1.85 ± 0.61	0.02 ± 0.01
CshA-ΔDD/CTD	–	ND	ND
	+RNA	2.93 ± 1.48	0.03 ± 0.02

ND, not determined.
[a]Stem-loop RNA with a 20-nt poly(A)3′ overhang (SL-A20) with a sequence of: AGUGCGGCAUGCAAGCUUGGCACUAAAAAAAAAAAAAAAAAAAA.
[b]$p < 0.0001$ between k_{cat} of CshA and CshA + RNA.

Collins et al., 2009; Jacewicz et al., 2014; Linden et al., 2008). To analyze the effect of RNA on ATP hydrolysis by CshA, we utilized an NADH-coupled steady-state method (Norby, 1988). ATP turnover was determined by measuring the rate of ATP hydrolysis as a function of ATP concentration in the presence and absence of SL-A20 RNA (Figure S6). CshA exhibited around 14-fold greater ATPase activity in the presence of RNA (k_{cat} = 1.28 s^{-1}) compared with the absence of RNA (k_{cat} = ~0.09 s^{-1}) (Table 2). These results are consistent with the turnover rates for Hera in the presence of various RNAs (k_{cat} values ranging from 1.3 to 2.6 s^{-1}) (Linden et al., 2008). Kinetic parameters of ATP hydrolysis for CshA-ΔCTD and CshA-ΔDD/CTD alone could not be determined due to no signal but, upon addition of RNA, k_{cat} values were approximately 0.02 and 0.03 s^{-1}, respectively (Table 2). Both CshA-ΔCTD and CshA-ΔDD/CTD exhibited a basal level of RNA-stimulated ATP hydrolysis activity, and this is consistent with our binding data showing that CshA-ΔCTD and CshA-ΔDD/CTD bind RNA more weakly in comparison with full-length CshA. The fact that the CshA-ΔCTD and CshA-ΔDD/CTD mutants exhibited RNA-dependent ATPase activity indicates that the CTD is not essential for activity, but that the CTD is required for significant enhancement of RNA-dependent ATP hydrolysis and would be essential for enzyme efficiency.

The K_m values for ATP binding of CshA-ΔCTD and CshA-ΔDD/CTD in the presence of RNA were around 1.85 and 2.93 mM, respectively. The K_m of CshA was around 0.78 mM in the absence of RNA and significantly improved to 0.16 mM in the presence of RNA, i.e., close to the value determined for CshA of *B. subtilis* (K_m = 0.225 mM) (Ando and Nakamura, 2006). The K_m and k_{cat} values for CshA were within the ranges observed for other DEAD-box proteins (Ando and Nakamura, 2006; Andreou and Klostermeier, 2014; Cao et al., 2011; Iost et al., 1999; Linden et al., 2008; Peck and Herschlag, 2003; Tsu and Uhlenbeck, 1998), whereas the truncation mutants exhibited weaker K_m and k_{cat}. These results suggest that RNA binding at the CTD enhances ATP binding, leading to greater ATP turnover.

CshA Cooperates with PNPase to Promote RNA Degradation

It has been shown that RhlB from *E. coli* directly interacts with PNPase forming a hetero-pentamer (Lin and Lin-Chao, 2005), but it remained unknown if CshA directly interacts with

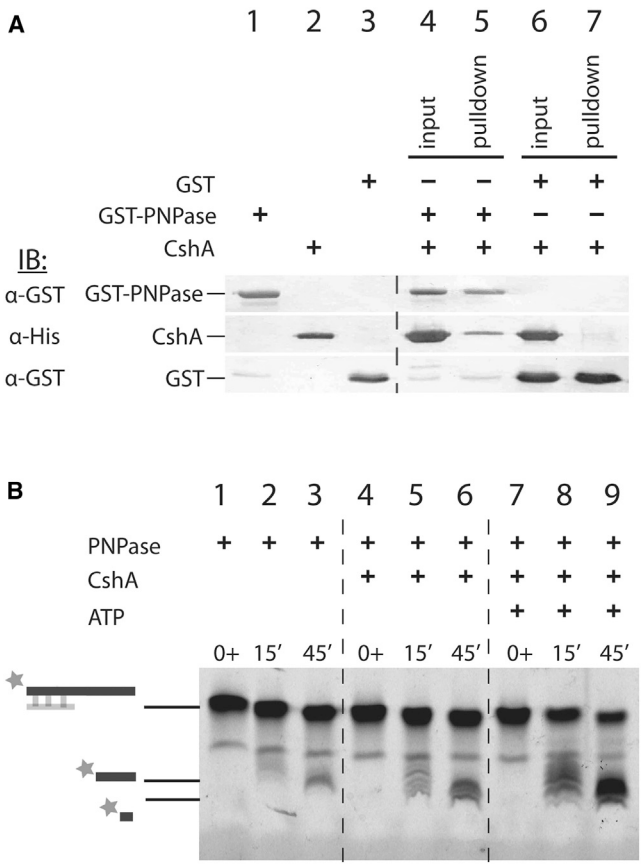

Figure 6. CshA Physically Interacts with PNPase to Promote Its Exoribonuclease Activity in Degrading Structured RNA
(A) Pull-down assays show that the GST-PNPase pulled down CshA (lane 5), but GST alone could not pull down CshA (lane 7).
(B) PNPase degradation of duplex RNA is enhanced in the presence of CshA and ATP. RNA substrates were prepared by annealing an 18-nt RNA labeled at the 5′ end with Cy3 (5′-Cy3-CCUCCCCCAAAAAAAAAA-3′) with an 8-nt RNA (5′-GGGGGAGG-3′) to generate a duplex RNA with a 10-nt 3′ poly(A) tail. The Cy3 are marked by gray stars. In the absence of CshA, degradation is minimal (lanes 1–3), while degradation increases slightly in the presence of CshA (lanes 4–6). Degradation of RNA by PNPase-CshA is greatly stimulated with ATP (lanes 7–9).

PNPase in the Gram-positive bacteria to promote RNA degradation. To test if CshA interacts directly with PNPase of *G. stearothermophilus*, we performed pull-down assays using recombinant N-terminal glutathione S-transferase (GST)-tagged PNPase (GST-PNPase) and C-terminal His-tagged CshA. GST-PNPase, CshA, and GST were expressed in *E. coli* and purified by chromatographic methods to high homogeneity as revealed by SDS-PAGE (Figure S1B). We found that CshA was pulled down by GST-PNPase, but not by GST alone (Figure 6A, lanes 5 and 7), suggesting that CshA interacts with PNPase in *G. stearothermophilus*.

We next conducted degradation assays to confirm the role of CshA in PNPase-mediated RNA degradation. We prepared a substrate by annealing an 8-nt RNA with an 18-nt RNA labeled with a Cyanine-3 at the 5′ end to generate an 8-base pair duplex RNA with a 10-nt poly(A)3′ tail. PNPase alone was able to degrade ssRNA substrates (Lin et al., 2012; Shi et al., 2008),

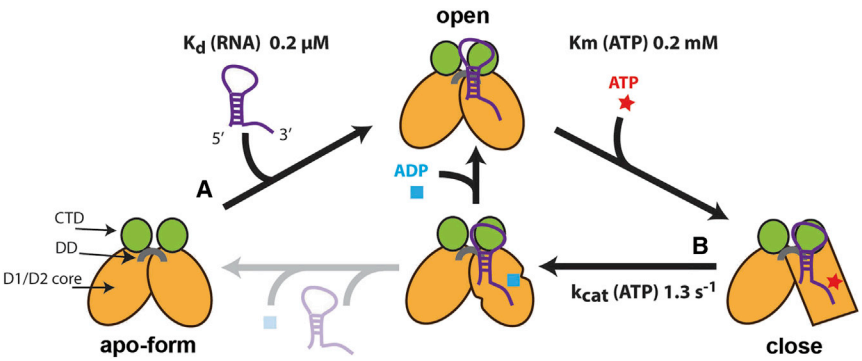

Figure 7. RNA-Unwinding Model by CshA

A schematic of CshA is shown where the orange oval represents the D1 and D2 domains, the gray half circle represents the dimerization domain, and the green circle represents the CTD. Kinetic parameters are taken from biochemical data (see Results). Path (A) shows binding of SL-A20 RNA to CshA defined by a K_d of 0.16 μM (CshA in the RNA-bound pre-unwound state illustrated by an oval). Subsequent binding of ATP (K_m = 0.2 mM) then allows a conformational change to the "close" conformation in the D1/D2 core resulting in local denaturation of the RNA base-paired region (CshA in the post-unwound state illustrated by a square). In path (B), RNA-bound CshA catalyzes ATP hydrolysis (k_{cat} = 1.3 s^{-1}), resulting in an ADP-bound state. After ADP is released, RNA may remain bound with CshA, which may enter another ATPase cycle.

but it could not degrade the duplex RNA region in the presence of Mg^{2+} in the time course experiments (Figure 6B, lanes 1–3). With the addition of CshA, the duplex RNA was slightly degraded by PNPase into smaller fragments (Figure 6B, lanes 4–6). The degradation by PNPase was greatly enhanced by addition of both CshA and ATP that generated smallest sizes of RNA fragments (Figure 6B, lanes 7–9). It is uncertain if PNPase directly interacts with CshA in the RNA degradation assays, but these results suggest that CshA unwinds duplex RNA in an ATP-dependent manner and the unwound RNA could be further degraded into small fragments by PNPase. Collectively, these results show that CshA physically interacts with PNPase and promotes the exoribonuclease activity of PNPase in degrading structured RNA in an ATP-dependent manner.

DISCUSSION

Here, we report the unique structure of a dimeric DEAD-box helicase, CshA. It has a distinctive V-shaped structure containing accessory DD and CTD domains in addition to the core RecA-like D1/D2 helicase core domains. This novel CTD domain exhibits RNA-binding activity in the sub-μM K_d range, and this binding does not depend on the presence of ATP or ADP. In contrast, both the dimeric CshA-ΔCTD and monomeric CshA-ΔDD/CTD exhibit RNA binding that is about one to two orders of magnitude weaker than the CTD alone and their binding is nucleotide dependent, as has been shown for the core D1/D2 domains of other DEAD-box proteins (Samatanga and Klostermeier, 2014). If RNA binding at the CTD and D1/D2 core were independent of each other, we would observe an apparent K_d for CshA equal to the K_d for CTD alone since RNA binding by the CTD alone is stronger than that of CshA-ΔCTD (for example the SL substrate). However, the full-length CshA exhibits the strongest RNA-binding activity, indicating that the CTD and D1/D2 cores cooperate in stabilizing RNA binding, especially RNAs containing secondary structures such as stem loops.

Combining the structural and biochemical data, we propose an RNA-unwinding model for the dimeric CshA (Figure 7). Although it is unclear exactly which part of the RNA is bound by the D1/D2 core, stoichiometric binding assays indicate that CshA binds one structured RNA substrate. Since ATP binding is tighter after RNA is bound (K_m = 0.16 mM versus K_m = 0.78 mM in the absence of RNA), CshA is likely to bind RNA initially (path A in Figure 7). In this RNA-bound pre-unwound state, binding of stem-loop RNA is stabilized by the CTD and D1/D2 core (the D1/D2 core is displayed in the pre-unwound state as an oval in Figure 7). This stabilization could involve the D2 domains of both protomers binding to the double-stranded stem-loop region, based on the structure of the D2 domain of Mss116 bound to double-stranded RNA showing that D2 interacts with both RNA strands of the double-stranded substrate (Mallam et al., 2012). It has been proposed that, upon ATP binding to Mss116, a closed conformation of D1/D2 is induced, which results in closing of the Va loop and "wedging" by a motif Ic helix that leads to extrusion of one strand of the double-stranded substrate (Mallam et al., 2012). Thus, upon ATP binding to CshA, a conformational change is induced resulting in base pair separation (the D1/D2 core in the post-unwound state is displayed as a square in Figure 7). The conformational changes of only the RNA-bound protomer are illustrated in Figure 7, as it remains unknown how the two CshA protomers work cooperatively in RNA binding and unwinding. In the post-unwound state, the resulting ssRNA interacts with the D1/D2 core of only one protomer, as this strand lies in the 5′ to 3′ orientation. The unwound single-stranded 3′ tail can be further degraded by 3′ to 5′ exoribonucleases, such as PNPase.

After both RNA and ATP are bound to CshA, ATP hydrolysis is followed as it is stimulated by RNA binding, and the production of ADP could result in release of both RNA and ADP to regenerate the apo-form of typical DEAD-box helicases. In this case, release of RNA renders the helicase non-processive. But different from the classical monomeric DEAD-box helicases, for the ADP-bound CshA, due to the presence of the CTD, the RNA may remain bound to CshA and, after release of ADP, the RNA-bound CshA can enter another ATPase cycle. As a result, when cooperating with ribonucleases, the dimeric CshA can unwind duplex RNA in a processive manner as RNA remain bound with CshA during ATP hydrolysis cycles. However, it should be noted that CshA is not a processive helicase as it cannot unwind a long duplex RNA by itself (data not shown). The CTD binds RNA irrespective of the nucleotide state and remains bound to the RNA even after its release by the D1/D2 core. In this regard, the function of the CTD is 2-fold: (1) to function with the D1/D2 core in stabilizing RNA binding and (2) to tether the RNA substrate while the

D1/D2 core cycles through ATP hydrolysis, resulting in continuous unwinding and release of the RNA substrate.

A recent study demonstrated that the CTD of CshA in *S. aureus* is important for mediating interactions with components of the degradosome, i.e., RNase J1/2, PNPase, and RNase Y (Giraud et al., 2015). This interaction region was mapped to the last 124 amino acid C terminus of CshA, which comprises part of the DD and CTD (Giraud et al., 2015). Although it is unclear whether the nucleases interact at the DD or CTD of CshA, this interaction would bring them physically close to any RNA bound at the CTD. Double-stranded RNAs could be directly cleaved by the endonuclease RNase Y into smaller fragments, which can then be unwound by CshA for more thorough cleavage by the exoribonucleases. How CshA functions with RNase Y, RNase J, and PNPase in denaturing large RNA structures for degradation remains unknown. Moreover, a previous study revealed that the DEAD-box helicase Ded1p functions as a homotrimer within which each protomer displays distinct roles in RNA binding and ATP hydrolysis (Putnam et al., 2015). How the two protomers in CshA cooperate in RNA unwinding also remains unknown and requires further investigation.

EXPERIMENTAL PROCEDURES

Cloning and Protein Expression

The full-length CshA gene of *G. stearothermophilus* was a generous gift from David Chwan-Deng Hsiao's laboratory, and the full-length CshA and its truncation mutant constructs (CshA-ΔCTD, residues 1–421; and CshA-ΔDD/CTD, residues 1–359) were cloned into pET22b vector using XhoI and NdeI restriction cutting sites to produce proteins with C-terminal 6xHistidine tags. All constructs were expressed in BL21(DE3) RIPL *E. coli* cells (Agilent Technologies) at OD_{600} of 0.6 with 0.5 mM isopropyl β-D-1-thiogalactopyranoside for 16 hr at 18°C, with the exception of CshA-ΔDD/CTD, which was induced for 4 hr at 37°C. Cells were harvested and lysed at 4°C in 50 mM Tris-HCl (pH 7.5), 500 mM NaCl, and 10 mM imidazole by microfluidizer (Microfluidics M-110P).

Crystallization and Structural Determination

CshA-ΔCTD was crystallized by the hanging-drop vapor diffusion method at room temperature. The protein crystal was grown in the crystallization drop made by mixing of 1 μL protein sample (10 mg/mL CshA-ΔCTD, 50 mM Tris-HCl [pH 8.0], 500 mM NaCl), and 1 μL reservoir solution (0.1 M sodium acetate and 1.5 M ammonium sulfate [pH 4.6]). X-ray diffraction data were collected at beamline 15A in the National Synchrotron Radiation Research Center in Hsin-chu, Taiwan. CshA-ΔCTD was crystallized in monoclinic a $P2_1$ unit cell with two molecules per asymmetric unit. The locations of the two protomers in the unit cell were determined by molecular replacement using YxiN of *B. subtilis* as the search model (PDB: 2HJV). The molecular model of the DD domain was built in the extra electron density in the difference Fourier maps using ARP/wARP software for initial model building. The final model was refined using CCP4, Refmac5. Crystallography statistics are shown in Table 1.

Small-Angle X-Ray Scattering

SAXS data were recorded at 37°C at SAXS beamline 23A coupled to a high-performance liquid chromatography system that was connected to the Agilent-Bio SEC-3 300 Å column in the National Synchrotron Radiation Research Center in Hsin-chu, Taiwan. A protein sample (486 μM CshA, 690 μM CshA-ΔCTD, or 161 μM CshA-ΔDD/CTD, all in 50 mM Tris-HCl [pH 7.5], 500 mM NaCl, and 10% glycerol) of 100 μL was injected into the Agilent-Bio SEC-3 column (300 Å pore size) at a flow rate of 0.02 mL/min and detected at a sample-to-detector distance of 3.2 m for CshA, 3.3 m for CshA-ΔCTD, and 3.1 m for CshA-ΔDD/CTD. An X-ray wavelength of 0.8266 Å and an energy of 15 keV were used for all samples. For CshA and CshA-ΔCTD, 40 frames of 30 s exposure each were collected, and for CshA-ΔDD/CTD, 24 frames of 30 s exposure each were collected. Each frame consisted of 0.01 mL of sample. Selected frames were merged and analyzed for initial R_g estimation by the PRIMUS program (Konarev et al., 2003) and by the GNOM program (Svergun, 1992) for D_{max} and P(r) distance distribution (ATSAS program suite, version 2.7) (Petoukhov et al., 2012). Molecular masses were determined using the ScÅtter Java-based application developed at the Diamond Light Source (UK) and the SIBYLS Beamline (USA) (Rambo, 2015). Low-resolution envelope structures were determined using ab initio programs DAMMIN (Svergun, 1999) or GASBOR (Svergun, 2001). A symmetry of P2 was set for CshA and CshA-ΔCTD and of P1 for CshA-ΔDD/CTD. The individual domains were manually placed into the envelope structures for visualization of the domain locations. Computation of the ensemble of CshA was conducted using the Ensemble Optimization Method (version 2.1, Tria et al., 2015).

ACCESSION NUMBERS

The accession number for the crystal structure of CshA-ΔCTD reported in this paper is PDB: 5IVL.

SUPPLEMENTAL INFORMATION

Supplemental Information includes Supplemental Experimental Procedures and six figures and can be found with this article online at http://dx.doi.org/10.1016/j.str.2017.01.012.

AUTHOR CONTRIBUTIONS

J.H., W.Z.Y., and B.G. performed the biochemical experiments. J.H., C.L.L., and W.Z.Y. collected X-ray diffraction data and determined the crystal structure. J.H. and H.S.Y. designed experiments, analyzed data, and wrote the manuscript.

ACKNOWLEDGMENTS

We would like to thank Ms. Evelyn Y.W. Huang for assistance in DNA cloning and protein purification, and Dr. Meng-Ru Ho and Dr. Meng-Chiao Ho for their assistance in conducting the FP assays at the Biophysics core center at the Institute of Biological Chemistry, Academia Sinica. Portions of this research were carried out at the National Synchrotron Radiation Research Center; a national user facility supported by the National Science Council of Taiwan. The Synchrotron Radiation Protein Crystallography Facility is supported by the National Core Facility Program for Biotechnology. Funding for open access charge: Academia Sinica, Taiwan.

Received: October 12, 2016
Revised: January 5, 2017
Accepted: January 29, 2017
Published: February 23, 2017

REFERENCES

Andersen, C.B., Ballut, L., Johansen, J.S., Chamieh, H., Nielsen, K.H., Oliveira, C.L., Pedersen, J.S., Seraphin, B., Le Hir, H., and Andersen, G.R. (2006). Structure of the exon junction core complex with a trapped DEAD-box ATPase bound to RNA. Science *313*, 1968–1972.

Ando, Y., and Nakamura, K. (2006). *Bacillus subtilis* DEAD protein YdbR possesses ATPase, RNA binding, and RNA unwinding activities. Biosci. Biotechnol. Biochem. *70*, 1606–1615.

Andreou, A.Z., and Klostermeier, D. (2014). eIF4B and eIF4G jointly stimulate eIF4A ATPase and unwinding activities by modulation of the eIF4A conformational cycle. J. Mol. Biol. *426*, 51–61.

Bernado, P. (2010). Effect of interdomain dynamics on the structure determination of modular proteins by small-angle scattering. Eur. Biophys. J. *39*, 769–780.

Borowski, L.S., Dziembowski, A., Hejnowicz, M.S., Stepien, P.P., and Szczesny, R.J. (2013). Human mitochondrial RNA decay mediated by

PNPase-hSuv3 complex takes place in distinct foci. Nucleic Acids Res. *41*, 1223–1240.

Cao, W., Coman, M.M., Ding, S., Henn, A., Middleton, E.R., Bradley, M.J., Rhoades, E., Hackney, D.D., Pyle, A.M., and De La Cruz, E.M. (2011). Mechanism of Mss116 ATPase reveals functional diversity of DEAD-Box proteins. J. Mol. Biol. *409*, 399–414.

Carpousis, A.J., Van Houwe, G., Ehretsmann, C., and Krisch, H.M. (1994). Copurification of *E. coli* RNAase E and PNPase: evidence for a specific association between two enzymes important in RNA processing and degradation. Cell *76*, 889–900.

Caruthers, J.M., Hu, Y., and McKay, D.B. (2006). Structure of the second domain of the *Bacillus subtilis* DEAD-box RNA helicase YxiN. Acta Crystallogr. Sect F Struct. Biol. Cryst. Commun. *62*, 1191–1195.

Chandran, V., Poljak, L., Vanzo, N.F., Leroy, A., Miguel, R.N., Fernandez-Recio, J., Parkinson, J., Burns, C., Carpousis, A.J., and Luisi, B.F. (2007). Recognition and cooperation between the ATP-dependent RNA helicase RhlB and ribonuclease RNase E. J. Mol. Biol. *367*, 113–132.

Coburn, G.A., Miao, X., Briant, D.J., and Mackie, G.A. (1999). Reconstitution of a minimal RNA degradosome demonstrates functional coordination between a 3′ exonuclease and a DEAD-box RNA helicase. Genes Dev. *13*, 2594–2603.

Collins, R., Karlberg, T., Lehtio, L., Schutz, P., van den Berg, S., Dahlgren, L.G., Hammarstrom, M., Weigelt, J., and Schuler, H. (2009). The DEXD/H-box RNA helicase DDX19 is regulated by an α-helical switch. J. Biol. Chem. *284*, 10296–10300.

Commichau, F.M., Rothe, F.M., Herzberg, C., Wagner, E., Hellwig, D., Lehnik-Habrink, M., Hammer, E., Volker, U., and Stulke, J. (2009). Novel activities of glycolytic enzymes in *Bacillus subtilis*: interactions with essential proteins involved in mRNA processing. Mol. Cell Proteomics *8*, 1350–1360.

Del Campo, M., and Lambowitz, A.M. (2009). Structure of the Yeast DEAD box protein Mss116p reveals two wedges that crimp RNA. Mol. Cell *35*, 598–609.

Eidem, T.M., Roux, C.M., and Dunman, P.M. (2012). RNA decay: a novel therapeutic target in bacteria. Wiley Interdiscip. Rev. RNA *3*, 443–454.

Fazala, F.M., Kosloverb, D.J., Luisi, B.F., and Blocka, S.M. (2015). Direct observation of processive exoribonuclease motion using optical tweezers. Proc. Natl. Acad. Sci. USA *112*, 15101–15106.

Giraud, C., Hausmann, S., Lemeille, S., Prados, J., Redder, P., and Linder, P. (2015). The C-terminal region of the RNA helicase CshA is required for the interaction with the degradosome and turnover of bulk RNA in the opportunistic pathogen *Staphylococcus aureus*. RNA Biol. *12*, 658–674.

Górna, M.W., Carpousis, A.J., and Luisi, B.F. (2012). From conformational chaos to robust regulation: the structure and function of the multi-enzyme RNA degradosome. Q. Rev. Biophys. *45*, 105–145.

Hardin, J.W., Hu, Y.X., and McKay, D.B. (2010). Structure of the RNA binding domain of a DEAD-box helicase bound to its ribosomal RNA target reveals a novel mode of recognition by an RNA recognition motif. J. Mol. Biol. *402*, 412–427.

Hardwick, S.W., Gubbey, T., Hug, I., Jenal, U., and Luisi, B.F. (2012). Crystal structure of *Caulobacter crescentus* polynucleotide phosphorylase reveals a mechanism of RNA substrate channelling and RNA degradosome assembly. Open Biol. *2*, 120028.

Henn, A., Bradley, M.J., and Cruz, E.M.D.L. (2012). ATP utilization and RNA conformational rearrangement by DEAD-Box Proteins. Annu. Rev. Biophys. *41*, 247–267.

Hogbom, M., Collins, R., van den Berg, S., Jenvert, R.M., Karlberg, T., Kotenyova, T., Flores, A., Karlsson Hedestam, G.B., and Schiavone, L.H. (2007). Crystal structure of conserved domains 1 and 2 of the human DEAD-box helicase DDX3X in complex with the mononucleotide AMP. J. Mol. Biol. *372*, 150–159.

Iost, I., Dreyfus, M., and Linder, P. (1999). Ded1p, a DEAD-box protein required for translation initiation in *Saccharomyces cerevisiae*, is an RNA helicase. J. Biol. Chem. *274*, 17677–17683.

Jacewicz, A., Schwer, B., Smith, P., and Shuman, S. (2014). Crystal structure, mutational analysis and RNA-dependent ATPase activity of the yeast DEAD-box pre-mRNA splicing factor Prp28. Nucleic Acids Res. *42*, 12885–12898.

Jarmoskaite, I., and Russell, R. (2014). RNA helicase proteins as chaperones and remodelers. Annu. Rev. Biochem. *83*, 697–725.

Karow, A.R., and Klostermeier, D. (2010). A structural model for the DEAD box helicase YxiN in solution: localization of the RNA binding domain. J. Mol. Biol. *402*, 629–637.

Klostermeier, D. (2013). Rearranging RNA structures at 75 degrees C? toward the molecular mechanism and physiological function of the *Thermus thermophilus* DEAD-box helicase hera. Biopolymers *99*, 1137–1146.

Klostermeier, D., and Rudolph, M.G. (2009). A novel dimerization motif in the C-terminal domain of the *Thermus thermophilus* DEAD box helicase Hera confers substantial flexibility. Nucleic Acids Res. *37*, 421–430.

Konarev, P.V., Volkov, V.V., Sokolova, A.V., Koch, M.H.J., and Svergun, D.I. (2003). PRIMUS - a Windows-PC based system for small-angle scattering data analysis. J. Appl. Crystallogr. *36*, 1277–1282.

Laalami, S., Zig, L., and Putzer, H. (2014). Initiation of mRNA decay in bacteria. Cell Mol. Life Sci. *71*, 1799–1828.

Lehnik-Habrink, M., Pfortner, H., Rempeters, L., Pietack, N., Herzberg, C., and Stulke, J. (2010). The RNA degradosome in *Bacillus subtilis*: identification of CshA as the major RNA helicase in the multiprotein complex. Mol. Microbiol. *77*, 958–971.

Lehnik-Habrink, M., Lewis, R.J., Mader, U., and Stulke, J. (2012). RNA degradation in *Bacillus subtilis*: an interplay of essential endo- and exoribonucleases. Mol. Microbiol. *84*, 1005–1017.

Lin, P.H., and Lin-Chao, S. (2005). RhlB helicase rather than enolase is the beta-subunit of the *Escherichia coli* polynucleotide phosphorylase (PNPase)-exoribonucleolytic complex. Proc. Natl. Acad. Sci. USA *102*, 16590–16595.

Lin, C.L., Wang, Y.T., Yang, W.Z., Hsiao, Y.Y., and Yuan, H.S. (2012). Crystal structure of human polynucleotide phosphorylase: insights into its domain function in RNA binding and degradation. Nucleic Acids Res. *40*, 4146–4157.

Linden, M.H., Hartmann, R.K., and Klostermeier, D. (2008). The putative RNase P motif in the DEAD box helicase Hera is dispensable for efficient interaction with RNA and helicase activity. Nucleic Acids Res. *36*, 5800–5811.

Linder, P., and Fuller-Pace, F. (2013). Looking back on the birth of DEAD-box RNA helicases. Biochim. Biophys. Acta *1829*, 750–755.

Linder, P., and Jankowsky, E. (2011). From unwinding to clamping – the DEAD box RNA helicase family. Nat. Rev. Mol. Cell Biol. *12*, 505–516.

Liou, G.G., Chang, H.Y., Lin, C.S., and Lin-Chao, S. (2002). DEAD box RhlB RNA helicase physically associates with exoribonuclease PNPase to degrade double-stranded RNA independent of the degradosome-assembling region of RNase E. J. Biol. Chem. *277*, 41157–41162.

Lorsch, J.R., and Herschlag, D. (1998). The DEAD box protein eIF4A. 1. A minimal kinetic and thermodynamic framework reveals coupled binding of RNA and nucleotide. Biochemistry *37*, 2180–2193.

Mallam, A.L., Jarmoskaite, I., Tijerina, P., Del Campo, M., Seifert, S., Guo, L., Russell, R., and Lambowitz, A.M. (2011). Solution structures of DEAD-box RNA chaperones reveal conformational changes and nucleic acid tethering by a basic tail. Proc. Natl. Acad. Sci. USA *108*, 12254–12259.

Mallam, A.L., Del Campo, M., Gilman, B., Sidote, D.J., and Lambowitz, A.M. (2012). Structural basis for RNA-duplex recognition and unwinding by the DEAD-box helicase Mss116p. Nature *490*, 121–125.

Mallam, A.L., Sidote, D.J., and Lambowitz, A.M. (2014). Molecular insights into RNA and DNA helicase evolution from the determinants of specificity for a DEAD-box RNA helicase. Elife *3*, e04630.

Mohanty, B.K., and Kushner, S.R. (2000). Polynucleotide phosphorylase functions both as a 3′ right-arrow 5′ exonuclease and a poly(A) polymerase in *Escherichia coli*. Proc. Natl. Acad. Sci. USA *97*, 11966–11971.

Norby, J.G. (1988). Coupled assay of Na+,K+-ATPase activity. Methods Enzymol. *156*, 116–119.

Oun, S., Redder, P., Didier, J.P., Francois, P., Corvaglia, A.R., Buttazzoni, E., Giraud, C., Girard, M., Schrenzel, J., and Linder, P. (2013). The CshA DEAD-box RNA helicase is important for quorum sensing control in *Staphylococcus aureus*. RNA Biol. *10*, 157–165.

Ozgur, S., Buchwald, G., Falk, S., Chakrabarti, S., Prabu, J.R., and Conti, E. (2015). The conformational plasticity of eukaryotic RNA-dependent ATPases. FEBS J. *282*, 850–863.

Pandiani, F., Chamot, S., Brillard, J., Carlin, F., Nguyen-the, C., and Broussolle, V. (2011). Role of the five RNA helicases in the adaptive response of *Bacillus cereus* ATCC 14579 cells to temperature, pH, and oxidative stresses. Appl. Environ. Microbiol. *77*, 5604–5609.

Peck, M.L., and Herschlag, D. (2003). Adenosine 5′-O-(3-thio)triphosphate (ATPgammaS) is a substrate for the nucleotide hydrolysis and RNA unwinding activities of eukaryotic translation initiation factor eIF4A. RNA *9*, 1180–1187.

Petoukhov, M.V., Franke, D., Shkumatov, A.V., Tria, G., Kikhney, A.G., Gajda, M., Gorba, C., Mertens, H.D., Konarev, P.V., and Svergun, D.I. (2012). New developments in the program package for small-angle scattering data analysis. J. Appl. Crystallogr. *45*, 342–350.

Putnam, A.A., Gao, Z., Liu, F., Jia, H., Yang, Q., and Jankowsky, E. (2015). Division of labor in an oligomer of the DEAD-box RNA helicase Ded1p. Mol. Cell *59*, 541–552.

Py, B., Higgins, C.F., Krisch, H.M., and Carpousis, A.J. (1996). A DEAD-box RNA helicase in the *Escherichia coli* RNA degradosome. Nature *381*, 169–172.

Rambo, R.P. (2015). Resolving individual components in protein-RNA complexes using small-angle X-ray scattering experiments. Methods Enzymol. *558*, 363–390.

Rambo, R.P., and Tainer, J.A. (2011). Characterizing flexible and intrinsically unstructured biological macromolecules by SAS using the Porod-Debye law. Biopolymers *95*, 559–571.

Rorbach, J., and Minczuk, M. (2012). The post-transcriptional life of mammalian mitochondrial RNA. Biochem. J. *444*, 357–373.

Roux, C.M., DeMuth, J.P., and Dunman, P.M. (2011). Characterization of components of the *Staphylococcus aureus* mRNA degradosome holoenzyme-like complex. J. Bacteriol. *193*, 5520–5526.

Rudolph, M.G., and Klostermeier, D. (2009). The *Thermus thermophilus* DEAD box helicase Hera contains a modified RNA recognition motif domain loosely connected to the helicase core. RNA *15*, 1993–2001.

Rudolph, M.G., and Klostermeier, D. (2015). When core competence is not enough: functional interplay of the DEAD-box helicase core with ancillary domains and auxiliary factors in RNA binding and unwinding. Biol. Chem. *396*, 849–865.

Russell, R., Jarmoskaite, I., and Lambowitz, A.M. (2013). Toward a molecular understanding of RNA remodeling by DEAD-box proteins. RNA Biol. *10*, 44–55.

Samatanga, B., and Klostermeier, D. (2014). DEAD-box RNA helicase domains exhibit a continuum between complete functional independence and high thermodynamic coupling in nucleotide and RNA duplex recognition. Nucleic Acids Res. *42*, 10644–10654.

Sengoku, T., Nureki, O., Nakamura, A., Kobayashi, S., and Yokoyama, S. (2006). Structural basis for RNA unwinding by the DEAD-box protein *Drosophila* vasa. Cell *125*, 287–300.

Shi, Z., Yang, W.Z., Lin-Chao, S., Chak, K.F., and Yuan, H.S. (2008). Crystal structure of *Escherichia coli* PNPase: central channel residues are involved in processive RNA degradation. RNA *14*, 2361–2371.

Steimer, L., Wurm, J.P., Linden, M.H., Rudolph, M.G., Wohnert, J., and Klostermeier, D. (2013). Recognition of two distinct elements in the RNA substrate by the RNA-binding domain of the *T. thermophilus* DEAD box helicase Hera. Nucleic Acids Res. *41*, 6259–6272.

Story, R.M., Li, H., and Abelson, J.N. (2001). Crystal structure of a DEAD box protein from the hyperthermophile *Methanococcus jannaschii*. Proc. Natl. Acad. Sci. USA *98*, 1465–1470.

Svergun, D.I. (1992). Determination of the regularization parameter in indirect-transform methods using perceptual criteria. J. Appl. Crystallogr. *25*, 495–503.

Svergun, D.I. (1999). Restoring low resolution structure of biological macromolecules from solution scattering using simulated annealing. Biophys. J. *77*, 2879–2886.

Svergun, D.I. (2001). Determination of domain structure of proteins from X-ray solution scattering. Biophys. J. *80*, 2946–2953.

Symmons, M.F., Jones, G.H., and Luisi, B.F. (2000). A duplicated fold is the structural basis for polynucleotide phosphorylase catalytic activity, processivity, and regulation. Structure *8*, 1215–1226.

Szczesny, R.J., Borowski, L.S., Malecki, M., Wojcik, M.A., Stepien, P.P., and Golik, P. (2012). RNA degradation in yeast and human mitochondria. Biochim. Biophys. Acta *1819*, 1027–1034.

Tria, G., Mertens, H.D.T., Kachala, M., and Svergun, D.I. (2015). Advanced ensemble modelling of flexible macromolecules using X-ray solution scattering. IUCr J. *2*, 207–217.

Tseng, Y.-T., Chiou, N.-T., Gogiraju, R., and Lin-Chao, S. (2015). The protein interaction of RNA helicase B (RhlB) and polynucleotide phosphorylase (PNPase) contributes to the homeostatic control of cysteine in *Escherichia coli*. J. Biol. Chem. *290*, 29953–29963.

Tsu, C.A., and Uhlenbeck, O.C. (1998). Kinetic analysis of the RNA-dependent adenosinetriphosphatase activity of DbpA, an *Escherichia coli* DEAD protein specific for 23S ribosomal RNA. Biochemistry *37*, 16989–16996.

von Moeller, H., Basquin, C., and Conti, E. (2009). The mRNA export protein DBP5 binds RNA and the cytoplasmic nucleoporin NUP214 in a mutually exclusive manner. Nat. Struct. Mol. Biol. *16*, 247–254.

Wang, D.D.-H., Shu, Z., Lieser, S.A., Chen, P.-L., and Lee, W.-H. (2009). Human mitochondrial SUV3 and polynucleotide phosphorylase form a 330-kDa heteropentamer to cooperatively degrade double-stranded RNA with a 3′-to-5′ directionality. J. Biol. Chem. *284*, 20812–20821.

Xiol, J., Spinelli, P., Laussmann, M.A., Homolka, D., Yang, Z., Cora, E., Coute, Y., Conn, S., Kadlec, J., Sachidanandam, R., et al. (2014). RNA clamping by Vasa assembles a piRNA amplifier complex on transposon transcripts. Cell *157*, 1698–1711.